journal of the mechanical behavior of biomedical materials 152 (2024) 106451

Contents lists available at ScienceDirect

Journal of the Mechanical Behavior of Biomedical Materials

journal homepage: www.elsevier.com/locate/jmbbm

Thermoplastic clear dental aligners under cyclic compression loading: A mechanical performance analysis using acoustic emission technique

Claudia Barile [a], Claudia Cianci [a], Vimalathithan Paramsamy Kannan [a], Giovanni Pappalettera [a,*], Carmine Pappalettere [a], Caterina Casavola [a], Carmela Suriano [b], Domenico Ciavarella [b]

[a] Dipartimento di Meccanica, Matematica e Management, Politecnico di Bari, Bari, Italy
[b] Dipartimento di Medicina Sperimentale e Clinica, Università di Foggia, Foggia, Italy

ARTICLE INFO

Keywords:
Clear dental aligners
Orthodontic forces
Cyclic test
Invisalign
Acoustic Emission
Optical microscopy

ABSTRACT

The objective of this work is to analyse the performance of clear aligners made of thermoplastic materials. Within this framework, the damage evolution stages and damage states of the aligners at different cycles of the compressive loading are evaluated using the Acoustic Emission (AE) technique. Three different clear aligner systems were prepared: thermoformed PET-g (polyethylene terephthalate glycol) and PU (polyurethane), and additively manufactured PU. Cyclic compression tests are performed to simulate 22500 swallows. The mechanical results show that the energy absorbed by the thermoformed PET-g aligner remains stable around 4 Nmm throughout the test. Although the PU-based aligners show a higher energy absorption of about 7 Nmm during the initial phase of the cyclic loading, this gradually decreases after 12500 cycles. The time-domain based, and frequency-based parameters of the stress wave acoustic signals generated by the aligners under compression loading are used to identify the damage evolution stages. The machine learning-based AE results reveal the initiation and termination of the different damage states in the aligners and the frequency-based results distinguish the different damage sources. Finally, the microscopy results validated the damage occurrences in the aligners identified by the AE results. The mechanical test results indicate that the thermoformed PET-g has the potential to match the performance and requirements of the dentistry of the popular Invisalign (additively manufactured PU). The AE results have the potential to identify at which cycles the aligners may start losing their functionality.

1. Introduction

1.1. Clear aligners for orthodontic treatment

The number of adults seeking orthodontic treatment connected with teeth crowding or maloccusion has increased significantly over the last 30 years (Barone et al., 2017; Buttke and Proffit, 1999; Elkholy et al., 2021). In fact, the number of adult patients with malocclusions is equal to, if not greater than, that of children and adolescents. However, a significant number of adult patients are reluctant to undergo traditional treatment with wires, bands, or brackets. A 1999 study shows that one of the main reasons for adult reluctance to undergo orthodontic treatment is the social acceptance of the less aesthetically pleasing traditional treatments (Buttke and Proffit, 1999). Apart from that, some studies have shown the adverse effects of the multifaceted oral environment on the wires and brackets (Eliades and Bourauel, 2005). For instance, the surface roughness of these components increases with the exposure to the oral environment, resulting in adverse effects on the treatment.

The applications of clear aligners (CA), particularly of thermoplastic materials, are well-known in dentistry as orthodontic retainers, temporomandibular joint splints, periodontal splints, mouth guards, and bleaching trays (Albilali et al., 2023; Fang et al., 2013; Gunatillake et al., 2003; Lombardo et al., 2015). CA have become a common orthodontic treatment practice over the years. The actual dental alignment of the patients is acquired by an intra-oral scanner and with the CAD/CAM systems and the CA are designed (Andjela et al., 2022; Barone et al., 2017; Schwitalla et al., 2015; Wang et al., 2019; Zhang et al., 2011). CA are used for a short period of time, typically between 7 and 14 days,

* Corresponding author.
E-mail address: giovanni.pappalettera@poliba.it (G. Pappalettera).

https://doi.org/10.1016/j.jmbbm.2024.106451
Received 19 December 2023; Received in revised form 26 January 2024; Accepted 30 January 2024
Available online 1 February 2024

during which a tooth or a group of teeth is programmed to move by smaller increments (0.1 mm–0.2 mm) or larger increments (0.5 mm–1.0 mm) (Elkholy et al., 2021; Rossini et al., 2015). The pre-planned increments allow the distribution of forces with constant gradual increments realign the misaligned teeth to the desired position over time (Boyd et al., 2000; Kravitz et al., 2009; Schuster et al., 2004).

Since the CA are replaced over a short period of time, they reduce the risks of periodontal disease such as gingivitis, and tooth decay and maintain oral hygiene (Quinzi et al., 2023). However, the thermoplastic materials are not entirely inert to the multifaceted oral environment. They are susceptible to deformation due to the masticatory forces and prolonged exposure to the salivary enzymes (which is debatable since it depends on the hydrophilic tendencies of the thermoplastic) (Fang et al., 2013; Lombardo et al., 2015, 2016; Pinchuk, 1995; Porojan et al., 2023). Moreover, the mechanical performance, dimensional stability, energy absorption and force delivery properties of the aligners are susceptible to changes depending on the type of manufacturing. Thermoplastic materials have the flexibility to be designed into complex shapes using several manufacturing methods (Dupaix and Boyce, 2005; Gunatillake et al., 2003; Iijima et al., 2015; Kohda et al., 2013; Lesser, 1995; Papadopoulou et al., 2019). Among them, thermoforming or layer-by-layer deposition using 3D printing methods are used for manufacturing CA. The impact of the occlusal forces on the dental aligners is influenced by their thickness and geometry (Casavola et al., 2022; Cianci et al., 2020). Therefore, it is essential to study the mechanical performance of the CA manufactured by thermoforming and Additive Manufacturing (AM)/3D printing under continuous orthodontic forces.

In recent years, several studies have reported the mechanical performance of different thermoplastic materials such as polyurethane and polyethylene terephthalate (PET-G, glycol modified), used for CA in the oral environment (Fang et al., 2013; Lombardo et al., 2015, 2016). However, most of these studies focus on the mechanical behaviour of the CA material rather than the aligner itself. Very few studies have addressed the effect of orthodontic forces on dental aligners (Albilali et al., 2023; Cianci et al., 2020; Kohda et al., 2013; Kravitz et al., 2009). Although these studies aimed at understanding the effect of the static forces on the dental aligners with different materials and thicknesses, to the authors' knowledge, a study of the effect of cyclic loading is rare (Cianci et al., 2020).

1.2. Non-Destructive evaluation of clear aligners

Indeed, the mechanical behaviour of CA is complex, which can be attributed to their geometrical irregularities and the complicated force delivered to each tooth, when they are loaded. It is, therefore, essential to seek for a more reliable tool for understanding their mechanical response. Passive Non-Destructive Evaluation (NDE) techniques are suitable for the understanding a mechanical behaviour of a component under constant load. Among the available NDE tools, the Acoustic Emission (AE) technique, which is a well-known passive NDE, can investigate the behaviour of a component throughout its entire loading history. The AE technique functions on the principle that elastic waves generated by a material or a component under load carries an information content on the status of the material. A component, in this case the CA, when stressed beyond a certain limit, it undergoes irreversible deformation by releasing a part of the stored strain energy. A portion of this relaxed strain energy propagates through the component as stress waves or a group of stress waves, which can be acquired by using piezoelectric transducers (Gillis, 1972; Hamstad, 2000; Liptai et al., 1972). The acquired stress waves/acoustic waves can be characterised in two different ways: parameter-based analysis and signal-based analysis. In parameter-based analysis, characteristic features of the stress wave signals in their time domain such as, rise time, rise angle, peak amplitude, RMS, counts, and so on are extracted and analysed. In the signal-based analysis, the signal features in their frequency or time-frequency domain are analysed. Both methods work on the fact that the damage source responsible for the stress wave generation can be characterised physically using these time domain- or frequency domain-based parameters (Barile et al., 2019; Saeedifar and Zarouchas, 2020). In principle, characterising the time-frequency characteristics of the stress waves may reveal information about their source. Within this research framework, the behaviour of the clear dental aligners under loading can be evaluated by studying the features of the stress waves generated during loading. Several researchers have illustrated the definitions of the AE wave features, their applications and their limitations in review articles and standard textbooks (Barile et al., 2020; Hamstad, 2000). However, the application of AE technique in dental applications is very limited. A research group (Li et al., 2011) used AE counts to monitor the interfacial debonding of dental composites used in restoration of cavities. Similar work was carried out by a researcher (Vallittu, 2002) to investigate the fracture characteristics of porcelain-fused-to-metal crown. Another research group (Ereifej et al., 2008) used the peak amplitude of the AE signals to investigate the load bearing capabilities of metal-free crowns. In the context of dental applications and AE technique, basic time-domain parameters such as peak amplitudes and counts are used for analysis. However, the AE technique has evolved in the medical and biomedical field over the years, where researchers have used advanced information-theoretic parameters such as entropy or complexity to define the characteristics of signal data in their time series (Abásolo et al., 2006; Aboy et al., 2006; Barile et al., 2023; Gusev et al., 1999; Radhakrishnan and Gangadhar, 1998), which have potential capability to be translated to AE signal data. Furthermore, several signal processing techniques, machine learning algorithms and artificial intelligence are frequency used to analyse the AE signal data over the years. For the sake of brevity, only a few numbers of techniques are highlighted here.

In this research work, the AE technique is used to investigate the mechanical behaviour of the CA under cyclic loading. Although the AE technique is commonly used in studying the mechanical behaviour of materials under cyclic loading, very limited work focuses on geometrically complex structures. One of the novelties of this research work lies in the application of AE technique for geometrically irregular CAs. Furthermore, an attempt has been made to characterise the damage states of these aligners by applying a machine learning algorithm, density-based data clustering, to the acquired AE data.

1.3. Research objective

Invisalign® is the most popular additively manufactured clear dental aligner, which has revolutionized the orthodontic treatments. They are prepared from a medical grade PU of commercial name SmartTrack™. The aim of this research work is to investigate and compare the mechanical behaviour of additively manufactured clear dental aligners with the thermoformed ones. Accordingly, these aligners are subjected to 22500 load-controlled compression cycles, while they are in constant contact with artificial saliva. Stress waves (or acoustic waves) generated by the aligners during the loading cycle are recorded and are used to characterize their mechanical behaviour. To the authors' knowledge, only a countable number of research articles are available in literature that have investigated the true mechanical behaviour of the CA. None of the articles have used any NDE tools for the same. The novelty of this research work not only rests in the utilization of AE technique for the mechanical characterisation of the CAs but also in integrating the machine learning algorithms in identifying the damage stages in the CAs under loading.

The article is organized as follows: Section 2 summarizes the details of the aligner, mechanical test methods and the AE data acquisition setup. Section 3 presents the cyclic test results, the optical microscopy, and the AE test results. The relation between the mechanical behaviour of the aligners and their AE results are discussed in Section 4. Section 5 presents the concluding statements of this research work.

2. Materials and methods

2.1. Preparation of test specimens

Original dental alignment record is a prerequisite for the preparation of aligners. An intra-oral scanner (TRIOS-3Shape) is used to acquire the digital dental alignment record of a patient. The scan output is processed by 3Shape OrthoAnalyzer® software to acquire the 3D reconstruction of the teeth with a permissible accuracy of 6.9 μm.

The additively manufactured CA is procured from Invisalign® by supplying the 3D dental alignment. The material data, other than the commercial name of the PU used, is not made available by the supplier.

For the production of thermoformed CA, first, a cast of the reconstructed dental alignment is additively manufactured from Daylight Hard Resin using Liquid Crystal HR2 3D Printer (Photocentric Ltd.). Clear PU and PET-g discs are thermoformed over the hard resin cast in Erokodent® Erkoform 3D vacuum machine. The discs are mounted on to the vacuum machine and heated by a medium-wave infrared heating unit. By applying a vacuum, the discs sheets are thermoformed over the cast.

Both these materials are of medical grade and are available commercially as sheets of uniform thickness (0.75 mm). The commercial name of the PU disc is Ghost Aligner, procured from Bart Medicals Ltd., and the PET-g is Essix ACE plastic, procured from Dentsply Sirona Inc.

The three CA tested in this study are named following their base material and the manufacturing process as T-PU, T-PET-G and AM-PU (T refers to the thermoforming process and AM refers to the additive manufacturing). All the aligners are passive ones, which means that they exactly reproduce the initial dental alignment of the patient, without causing any tooth movement.

For simulating the multifaceted oral environment, artificial saliva is made to be in contact with the aligner throughout the compression cyclic tests (Eliades and Bourauel, 2005). The chemical composition of the artificial saliva is presented in Table 1, and the application process is explained in the subsequent sections.

2.2. Test methods – cyclic loading

In order to apply the mechanical load, upper and lower hard resin casts are also prepared. The upper and lower casts are mounted on an INSTRON 3344 single-column universal testing machine equipped with a 1 kN loading cell. This electro-mechanical testing machine is controlled by INSTRON Bluehill 2.5 software, which records the displacement and force information. The upper and lower casts are held firmly at a constant pressure of 10 MPa by a pneumatically operated end-grips. The casts are designed and aligned in a way to simulate the occlusal force during the masticatory function. The clear dental aligner is placed on the upper cast before the compressive load is applied. Cyclic compression tests are performed in a load-controlled mode at a constant cyclic load frequency of $= 0.25\ cycles\ s^{-1}$.

During the first stage of the loading cycle, the compressive load is ramped from 0 to 50 N in 1s. The load 50 N is selected as the nominal occlusal force exerted by a human during opening and closing of the jaw during swallowing operation (Duyck et al., 2000; Gibbs et al., 1981; Tak et al., 2023). In the second stage, the dwell time of 1s is chosen to simulate the maximum occlusal contact duration during swallowing. In the third stage, the compressive load is ramped down to 0 N in 1s and the final stage of the cycle is another dwell of 1s. As previously mentioned, the cyclic tests are repeated for 22500 cycles, calculated on the basis of number of the occlusal contacts during swallowing act in the period of use of the aligner, on average equal to 15 days.

To simulate the oral environment, a sponge is impregnated with the artificial saliva and is placed between the upper and lower cast, ensuring its contact with the aligner. The setup is enclosed by a cellulose hydrate film to prevent the evaporation of the saliva during the test. The experimental setup of the upper and lower cast with the aligner and the final test setup are provided in Supplementary Materials (Figs. S1(a) and S1(b)).

The mechanical data, displacements and the applied loads are recorded at a sampling rate of 20 Hz. The tests are carried out uninterrupted at room temperature and under atmospheric ambient conditions.

Table 1
Chemical composition of artificial saliva.

Composition	Content (%)
Sorbitol[a]	4.3
KCl	0.12
NaCl	0.085
E218[b]	0.05
$CaCl_2$. $2H_20$	0.013
K_2HPO_4	0.013
$MgCl_2$	0.005
Water	Balance

[a] Sugar Alcohol – $C_6H_{14}O_6$.
[b] Methylparaben – $C_8H_8O_3$.

2.3. Test methods – AE data acquisition setup

To record the acoustic waves generated by the dental aligners under cyclic loading, a piezoelectric sensor is used. The sensor is a lightweight miniature PICO sensor (Physical Acoustics) with an operating frequency of up to 750 kHz and resonant frequencies of 250 kHz and 550 kHz. The sensor is placed on the upper cast, close to the third right molar position. It is recommended that the sensor must be placed on a flat surface to ensure good acoustic coupling. Due to the complex geometry of the aligner, only the above position is sufficiently flat to mount the sensor in accordance with the recommendation (Barile et al., 2020). A thin layer of silicone grease is applied between the surface of the sensor and the cast to prevent the acquisition of reverberation frequencies. The sensor is clasped to the cast with a clip to ensure a uniform pressure during the coupling. During AE data acquisition, the acquisition threshold, preamplification of the recorded signals and analogue filters are of paramount importance. However, for a complex geometry such as a dental aligner, there are no recommended or available standard methods. Therefore, a preliminary analysis is performed to set the AE acquisition parameters.

First, a previously tested dental aligner (a thermoformed PET-G clear aligner) is loaded onto the test setup (Casavola et al., 2022; Cianci et al., 2020). This dental aligner had a visible crack at the first third molar position. A compressive load of 100 N is then applied rapidly to augment the crack length. This is followed by a cyclic compression test for 100 cycles similar to the load cycle explained in Section 2.1. However, the compressive load is ramped up to 75 N, instead of 50 N during this preliminary analysis. The purpose of this test is to promote the crack growth in the dental aligner. The propagation of the crack growth generated AE signals, which are recorded by the piezoelectric sensor.

During the course of this preliminary test, the AE acquisition parameters are set by trial and error. With an acquisition threshold of 26 dB, preamplification of 60 dB and analogue filters of 100 kHz/1 MHz, the AE signals from the crack events are recorded free from interference of the test machine and other sources. The signals are acquired under burst-mode of acquisition, the AE signals of length 2K are registered using an 18-bit 40 MHz A/D system, PAC PCI-II Data Acquisition System (Physical Acoustics, MISTRAS).

The general distribution of the AE data that can be expected during the crack growth in the dental aligners can be viewed in the Supplementary Fig. S2. The distribution of the AE signals in terms of their peak amplitude and peak frequency in the Fast Fourier Transform (FFT) spectrum is provided in the Supplementary Fig. S3.

Through this preliminary analysis, it is understood that the frequency components of the AE signals from crack growth event will have

peak frequencies starting from 100 kHz and mostly centred around 200 kHz. The peak amplitude distribution of the signals, however, will depend on the crack location and the amount of energy released during the crack propagation.

The frequency characteristics of the AE signals will be discussed in the subsequent sections.

2.4. AE signal data analysis

In order to identify the damage states of the CAs during the cyclic loading, the AE signal data is classified using density-based data clustering, a machine learning algorithm. To efficiently use the AE data, a parameter-based feature and a signa-based feature are taken for clustering the AE signals in different groups. The peak frequency of the AE signals, as understood from the previous section, is taken as the signal-based feature. The energy of the AE signals is taken as the parameter-based feature. Energy of the AE signals has been successfully used by several researchers in characterizing crack propagation in composites (Baker et al., 2015), metals (Aggelis et al., 2011; Huang et al., 2023), and concrete (Burud and Kishen, 2021; Ohno and Ohtsu, 2010). Considering their effectiveness in identifying the damage progression, these two features are taken for analysis.

Density-based spatial clustering of applications with noise (DBSCAN) is used for clustering the selected AE features. Considering the duration of the cyclic compression test, it is hypothesized that the different damage states may result in producing a large amount of AE signal data. Furthermore, a large spatially distributed data with noise/outliers can be expected in such case. DBSCAN is designed to discover the clusters and noise in data by identifying the core points, border points, and noise points based on the pairwise distance between the datapoints. For the sake of brevity, the algorithm is not explained here; it is well-documented in literature and can be found elsewhere (Ester et al., 1996; Huang et al., 2023; Sander et al., 1998).

In this research work, the DBSCAN function available in the Statistics and Machine Learning Toolbox of MATLAB® 2022 is used.

2.5. Optical microscopy

The inner surface of the dental aligners, after the cyclic loading, are tested under Optical Microscopy (NIKON SMZ800). The aligners are cleaned properly with acetone to remove the foreign particles before scanning them under the optical microscope.

3. Results

3.1. Cyclic compression test results of clear dental aligners

The mechanical behaviour of the aligners is studied using the hysteresis curves obtained from the load-displacement curves. The hysteresis curves of T-PET-G, T-PU and AM-PU are presented in Fig. 1(a) and (b) and 1(c), respectively. Three representative hysteresis curves from three phases of the tests are presented here. Cycles 2, 100 and 500 are provided as representatives of the initial phase (which occur in the first hour of loading), cycles 5000, 75000 and 10000 for the mid-phase and cycles 15000, 20000 and 22499 (final hours of loading) for the final phase of the tests.

All three aligners show a bilinear response during the loading in the initial phases of the tests. However, there are distinguishable differences in the displacement of the bilinear response. In Cycle 2, the maximum load response is reached at a displacement of 0.51 mm for T-PET-G (Fig. 1(a)), while the displacement is 0.94 mm and 1.08 mm for T-PU and AM-PU (Fig. 1(b) and (c)). The bilinear stiffening changes of the load response in this cycle occur at 0.36 mm, 0.78 mm and 0.90 mm, respectively for the three aligners in order. The load at the stiffening change is also lower for T-PET-G, which is 13 N, as opposed to 28 N and 24 N for T-PU and AM-PU. The unloading paths show a large hysteresis, with the size of the hysteresis being much larger for AM-PU, relatively smaller for T-PU and much smaller for T-PET-G. The size of the hysteresis path may indicate the amount of energy absorbed by the aligners, which is greater for AM-PU and much less for T-PET-G. This can be attributed to the large deformation of PU compared to that of PET-g. The size of the hysteresis curve in the unloading phase indicates the softening behaviour of the material, which is again high for the PU aligners than that of the PET-g one.

In Cycle 100, the displacements at maximum load, displacement at bilinear changes and their respective loads for all the three aligners do not exhibit any significant changes from cycle 2. Similarly, the load-displacement responses for Cycle 500 also do not show any significant variations from Cycle 2. This indicates that the mechanical responses of the aligner, despite their individual differences, do not show any significant changes during the initial loading phase.

The load-displacement curves of the aligners during the middle phase of the cyclic tests at cycles 5000, 7500 and 10000 are presented in Fig. 1 as discontinuous lines. The first significant difference between the curves in the initial phase and the middle phase is the change in the initial displacements of the hysteresis curves, which have shifted by approximately 0.2 mm from the initial position in T-PU (see Fig. 1(b)) and AM-PU (see Fig. 1(c)). As the tests are load-controlled, it is reasonable to assume that the change in displacement could be related to the amount of energy absorbed by the aligner resulting in a residual deformation and its stiffness in the loading and unloading phases. Once again, the residual deformation of T-PU and AM-PU are slightly larger than their counterpart, which indicates their larger deformation. However, there are no major changes in the displacement at maximum load.

In T-PET-G, there is a clear change in the bilinear stiffening in cycle 5000 (see Fig. 1(a)). The displacement at which the bilinear load response changes from 0.36 mm in the initial phases to 0.40 mm in cycle 5000. Moreover, the load at which the change occurs has increased from 13 N in the initial phases to 31 N. The unloading phase is also characterized by a relatively larger hysteresis. This observation is also found in the cycles 7500. The displacement at the elbow of the bilinear load response in T-PU and AM-PU (see Fig. 1(b) and (c), respectively) also have changed to 0.83 mm and 0.94 mm in the cycles 5000, 7500 and 10000. However, there is no significant changes in the load at the elbow of the bilinear changes. The overall indication for the middle phase of the aligners is that the energy absorbed has increased for T-PET-G, while it has decreased for T-PU and AM-PU in the middle phase.

Cycles 15000, 20000 and 22499 are taken to analyse the final stages of loading. The initial displacement positions of T-PU and AM-PU have shifted further to 0.4 mm as opposed to 0.2 mm in the middle phase. As indicated earlier, this residual deformation is the indication of large deformation in the material. The aligners made from PU, regardless of their manufacturing routine, continuously undergo large deformations over the cycles. This increasing trend is particularly evident when comparing the load curves of Cycle 15000 and Cycle 20000. T-PET-G, however, has not shown any difference in the initial displacement. Nonetheless, the bilinear load response has changed into a more or less linear response (with no obvious elbow at the change) in this stage. The unloading phase in T-PET-G is quite similar to the middle phase.

There is a major difference in the load-displacement curve in the T-PU. In Cycles (20000 and 22449, the unloading curve is characterized by a smaller hysteresis, indicating that the total energy absorbed by the T-PU is very low in the final phase of the cyclic test.

Furthermore, to evaluate the variation in the mechanical responses of the aligners at different phases of the cyclic test, the energy absorbed, and the stiffness are calculated from the load-displacement curve and are reported in Fig. 2. The energy absorbed is calculated by integrating the area covered by the hysteresis curve and is reported in Fig. 2(a). The stiffnesses are calculated for the bilinear responses by taking their respective slopes and are reported as Stiffness – Slope 1 and Stiffness – Slope 2 in Fig. 2(b) and (c), respectively.

The energy absorbed by the aligners during the cyclic test follows the

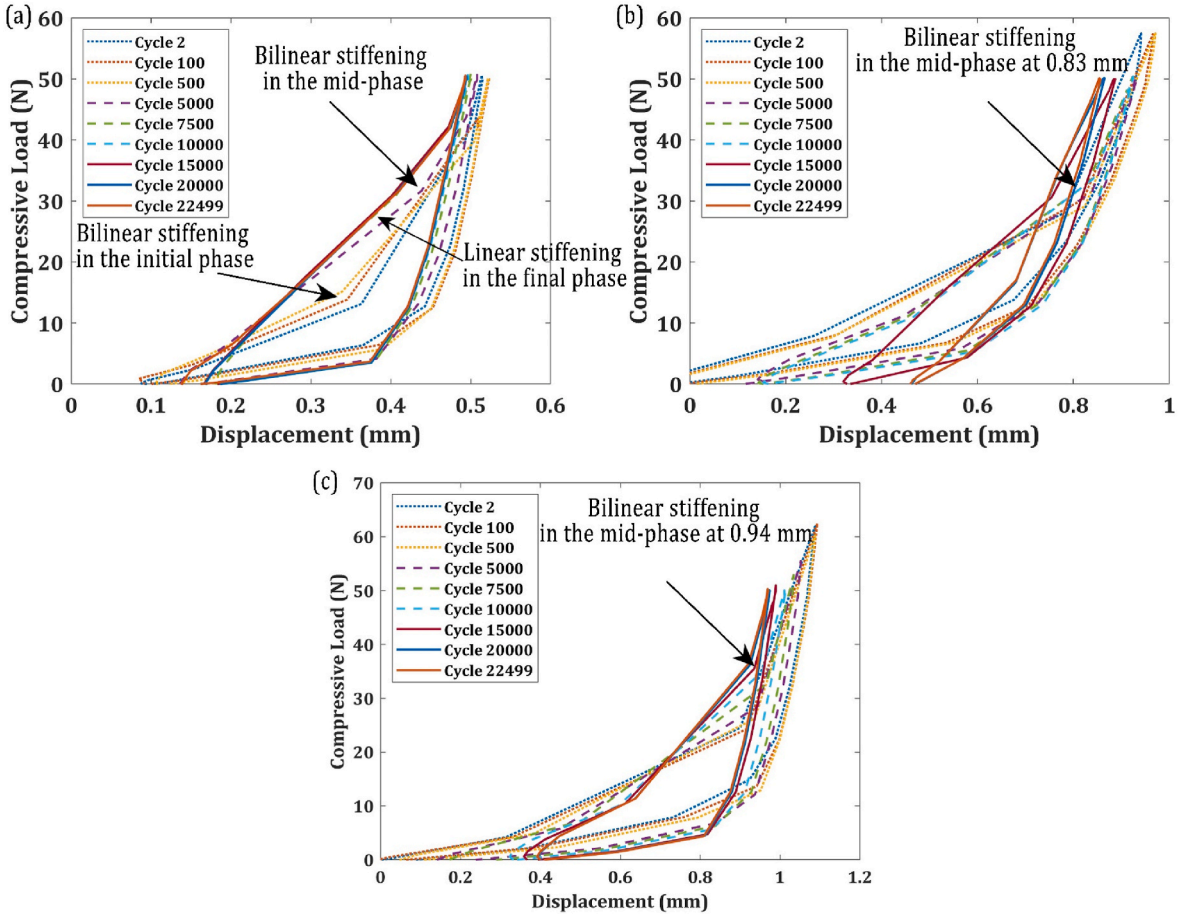

Fig. 1. Load-Displacement Curves of the Cyclic Loading in (a) T-PET-G; (b) T-PU and (c) AM-PU (In the coloured version of the figure, initial phase is plotted in dotted lines, mid-phase in discontinuous lines and final phase in solid lines).

trend described in this section. The T-PET-G absorbed the least energy (approximately 4 Nmm) in the initial phase, increased slightly in the middle phase and maintained its energy absorption characteristics for the rest of the loading cycles. On the other hand, although the T-PU has higher energy absorption in the initial phase (around 7 Nmm) compared to T-PET-G, there is a decrease in the middle phase where it drops to an average of 6 Nmm. After 10000 cycles, the energy begins to decrease gradually in the final phase, dropping suddenly from 5.1 Nmm to 2.6 Nmm in the final phases. This indicates some sudden changes in the mechanical response of the T-PU in the final phase of the test. The AM-PU has the highest energy absorption in the initial phase (7.8 Nmm), and this gradually decreases over the duration of the test. Although the energy absorption seems to increase in the middle phase from 2000 cycles to 6000 cycles, it gradually decreases again. Nevertheless, the energy absorbed by AM-PU in the last cycle 22499 is 6.49 Nmm, which is significantly higher than the average energy absorbed by T-PET-G and T-PU.

The stiffness of the aligners is reported in Fig. 2(b) and (c). Despite the differences in the stiffness values calculated from the two slopes of the bilinear load responses, their trends are more or less similar. T-PET-G, contrary to its energy absorption characteristics, has the highest stiffness. This can be attributed to the initial displacement in the load-displacement curves, which influences the stiffness slopes, at different phases of the cyclic loading, which did not vary significantly. On the other hand, the stiffness of the T-PU has increased significantly in the final phase of the test. In fact, it starts to increase rapidly around 16000 cycles, where there was a rapid energy drop (See Fig. 2(a)). Analogous to the energy absorption curve, the stiffness curve of AM-PU has gradually increased over the duration of the test.

3.2. Optical microscopy results

Optical microscopy is used to analyse different dental positions of the aligners after cyclic loading of 22500 cycles. The dental positions are notated based on ISO 3950 – Designation System for Teeth and Areas of Oral Cavity. The dental positions from the maxillary right central incisor, mandibular incisor up to the maxillary third molar are sequentially numbered as 11, 12, …18, respectively and the left part is numbered as 21, 22, …28.

A few microscopic images of the untested dental aligners are presented in the Supplementary Fig. S4. A few areas of strain hardening (with beachmarks and whitening) and cracks less than 1 mm in length can be found in the untested T-PU aligners. These are likely to be the result of thermoforming process, and therefore, the cracks less than 1 mm in length are referred to as ‘minor cracks’ throughout this section.

The microscopic images of the tooth positions where damages occurred are presented in this section. Fig. 3 shows the microscopic images of the teeth 14, 18, 26 and 27 of T-PET-G. No major damage is observed in this aligner. Only one major crack 1.32 mm in length can be found in tooth 14 (see Fig. 3(a)) and very few minor cracks are observed in the same tooth position. A minor crack 0.62 mm in length can be found in tooth 26 (see Fig. 3(c)). In tooth 27, a small chip approximately 0.23 mm in diameter is removed from the aligner. Otherwise, there is no significant damage in T-PET-G. A few areas of strain hardening can be observed, particularly in tooth 18 (see Fig. 3(b)), but it is unclear whether this is due to the thermoforming or the cyclic compression. Some other minor cracks and areas of strain hardening regions are observed in Teeth 17 and 21.

Fig. 4 shows the microscopic images of T-PU at positions 17, 18, 21

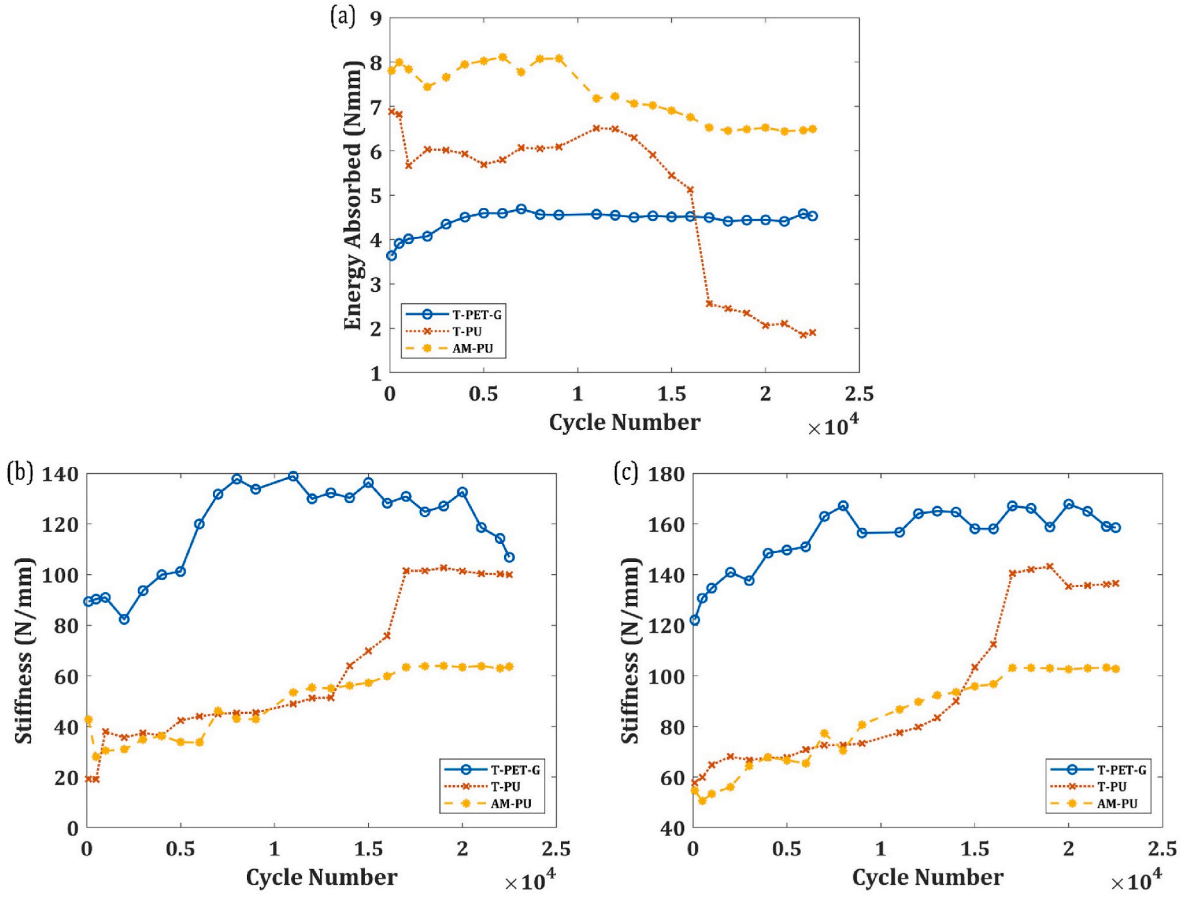

Fig. 2. (a) Energy absorbed by the Clear Dental Aligners during the Cyclic Compression Test and their Stiffness calculated from (b) First Linear Slope and (c) Second Linear Slope of the Load-Displacement Curves.

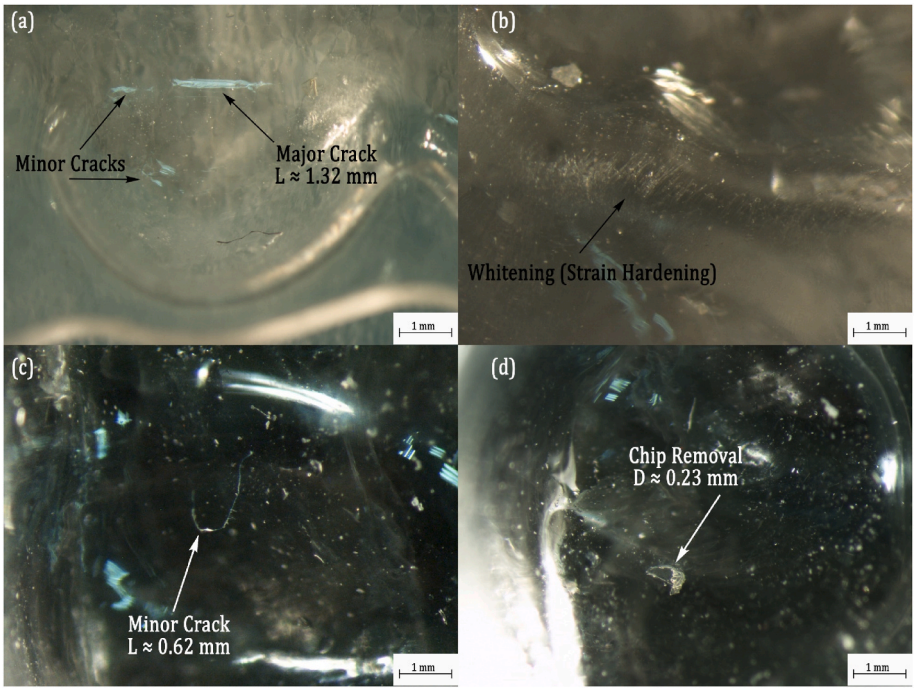

Fig. 3. Microscopic Images of T-PET-G taken from different Dental Positions (a) Tooth 14; (b) Tooth 18; (c) Tooth 26 and (d) Tooth 27.

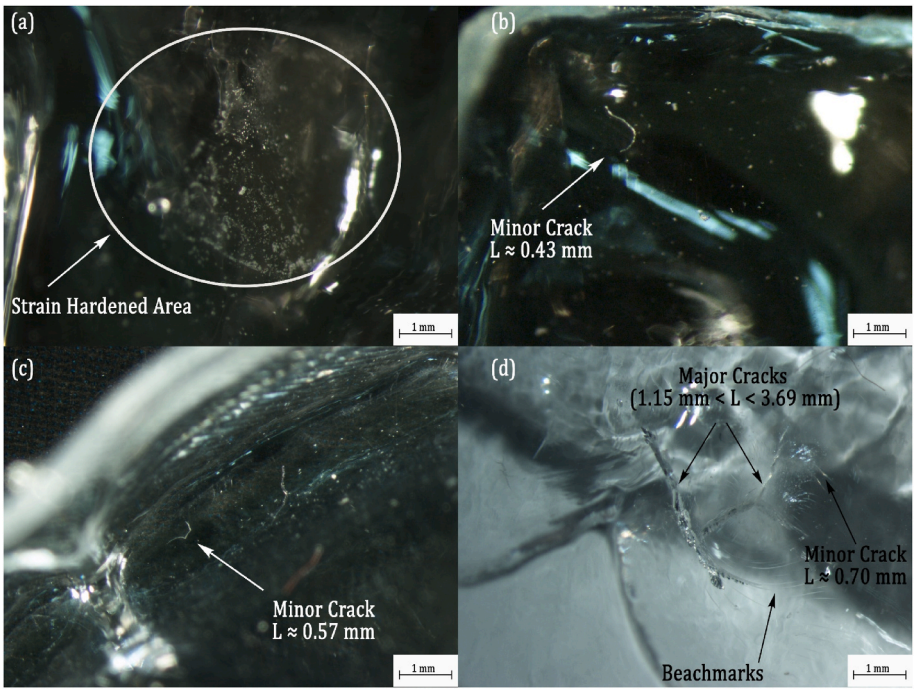

Fig. 4. Microscopic Images of T-PU taken from different Dental Positions (a) Tooth 17; (b) Tooth 18; (c) Tooth 21 and (d) Tooth 27.

and 27. Similar to T-PET-G, a few minor cracks approximately 0.50 mm in length are observed in two different dental positions, Teeth 18 and 21 (See Fig. 4(b) and (c), respectively). A local strain hardened area can be observed in Tooth 17 (See Fig. 4(a)). Interestingly, a significant number of localized damages can be observed in Tooth 27 in Fig. 4(d). Large cracks with lengths exceeding 3.50 mm can be observed in this tooth position. Furthermore, these cracks originate from a confined position and grow along the strain hardened regions. In the vicinity of these major cracks several minor cracks and locally strain hardened areas can be found.

Since there are no microscopic damages observed in the AM-PU aligner, their microscopic images are presented in the supplementary file as Fig. S5.

3.3. Acoustic Emission Results

The AE technique can provide a deeper insight into this. For instance, it can provide in-situ information such as the duration of the initiation and termination of damage (chip formation or crack nucleation) and possibly distinguish between the different damage sources.

The AE data acquired during the cyclic tests are analysed in two modes: parameter-based analysis and signal-based analysis. In parameter-based analysis, the counts of the AE signals recorded during the cyclic tests are taken and compared with the energy absorbed by the aligners. The count is the number of instances the recorded amplitude of the AE signal exceeds the detection threshold. In order to improve the signal-to-noise ratio of the acquired data and to use the more relevant data for analysis, the acquired signals are filtered again after acquisition with a threshold of 35 dB. A question may arise why the detection threshold is not directly assigned at 35 dB instead of 26 dB to avoid this second filtering. The acquisition of AE signals by the data acquisition system depends on several factors such as Peak Definition Time, Hit Detection Time and Hit Lockout Time (their definitions can be found elsewhere [29–31]). It is possible to lose relevant information if the detection threshold is set to a lower value. For this reason, an initial analysis was carried out to set the detection threshold and the acquired data during the cyclic tests are filtered by 35 dB. It should be noted that no AE signals are detected from AM-PU. There are two reasons for this: First, there is no damage such as chip formation or crack nucleation in AM-PU (See Fig. S5; which will be explained in Section 4); second, if there were some energy releases due to damage, they would have generated acoustic waves with amplitude below the detection threshold. Since there are only minor cracks and a very little chip formation in AM-PU (See the supplementary file Fig. S5), it can be concluded that these damage sources did not generate AE signals above the detection threshold. Therefore, the results of T-PET-G and T-PU are reported in this section.

For the parameter-based analysis, the cumulative counts of the AE signals recorded during the tests of the aligners T-PET-G and T-PU are plotted over their respective energy absorption characteristics in Fig. 5 (a) and (b), respectively.

Based on the trend of the cumulative counts in Fig. 5, AE signals from different cycles of the mechanical loading are taken for analysis. The frequency characteristics of AE signals from different cycles are presented in Fig. 6. Fig. 6 distinctly shows the FFT of the signals from T-PET-G at cycles 4000 to 9000 (in Fig. 6(a)) and cycles 18000 to 20000 (in Fig. 6(b)) and from T-PU at cycles 2000 to 5000 (in Fig. 6(c)) and cycles after 10000 (in Fig. 6(d)). The reason for selecting these specific cycles will be explained in detail in Section 4, but the general idea is to analyse the signals from specific cycles where the damages occurred in T-PET-G and T-PU aligners.

The AE features of the signals, the energy and peak frequency, generated by T-PET-G and T-PU are clustered using DBSCAN and their results are presented in Fig. 7(a) and (b), respectively.

In Fig. 7(a), based on their density distribution, the AE signals from T-PET-G are classified into two different groups: Group 1 having peak frequencies between 100 kHz and 200 kHz and Group 2 having peak frequencies between 600 kHz and 700 kHz. Apart from those two groups, there are some outliers in the data distribution. While in Fig. 7 (b), the AE signals from T-PU are classified into four groups, excluding the outliers. The frequency distributions of these groups strictly lie within the 100 kHz and 200 kHz frequency band however, their distribution varies based on both the peak frequencies and their energies. Group 1 signals have frequencies below 125 kHz and their energies are less than 2 aJ. Group 2 signals have frequencies between 175 kHz and 200 kHz, while their energies are less than 1.5 aJ. Group 3 signals have

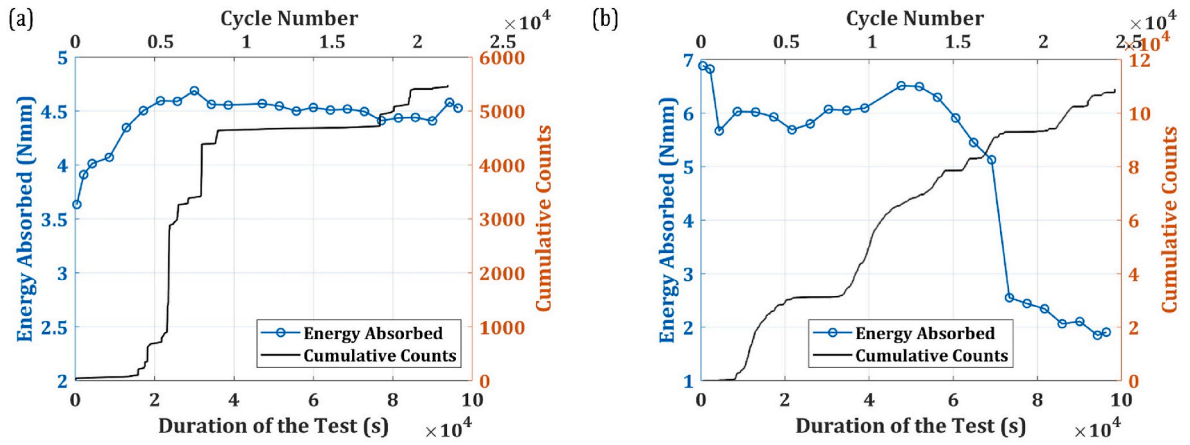

Fig. 5. Comparison of the mechanical behaviour and the acoustic Emission results: Energy absorbed by the aligner and cumulative counts of the AE events of (a) T-PET-G and (b) T-PU dental aligners.

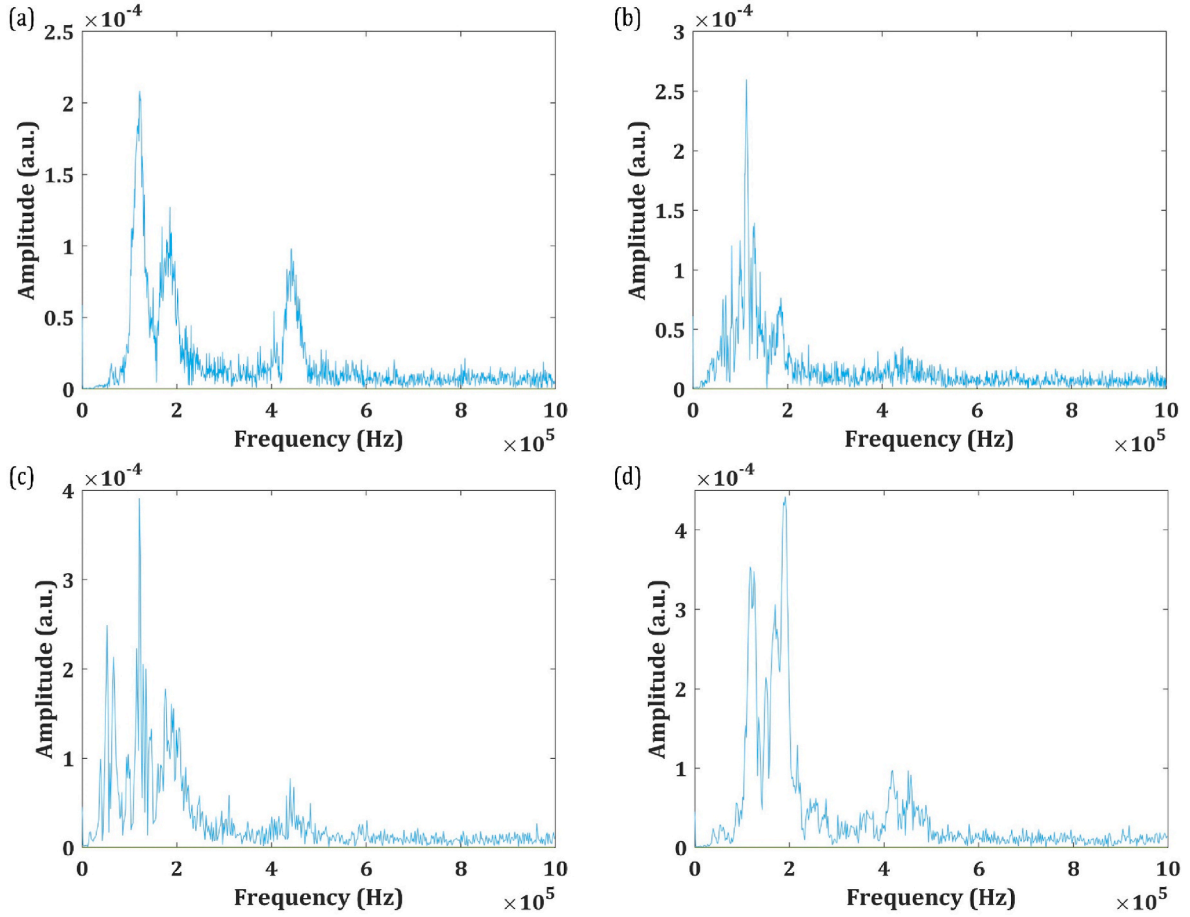

Fig. 6. FFT of the AE Signals generated from T-PET-G in (a) Cycles 4000 to 9000; (b) Cycles 18000 to 20000 and FFT of the AE Signals from T-PU in (c) Cycles 2000 to 5000; (d) After Cycle 10000.

frequencies between Groups 1 and 2, however, their energies are quite low (typically less than 1 aJ). Group 4 signals exhibit unique characteristics in terms of their energies which are greater than 6.5 aJ.

The temporal distributions of the classified AE signals from T-PET-G and T-PU are presented in Fig. 8(a) and (b), respectively.

These results will be discussed in the next section.

4. Discussion

Upon observing the results of the cyclic tests in Figs. 1 and 2, two important questions need to be answered: What might be the reason for the sudden energy drop accompanied by the increase in stiffness in PU-based aligners? What might be the significance of this mechanical response? Theoretically, energy is absorbed due to the plastic deformation in the aligner during the cyclic tests (Qi and Boyce, 2005; Ryu et al., 2018; Tamburrino et al., 2020). The increase in energy in the

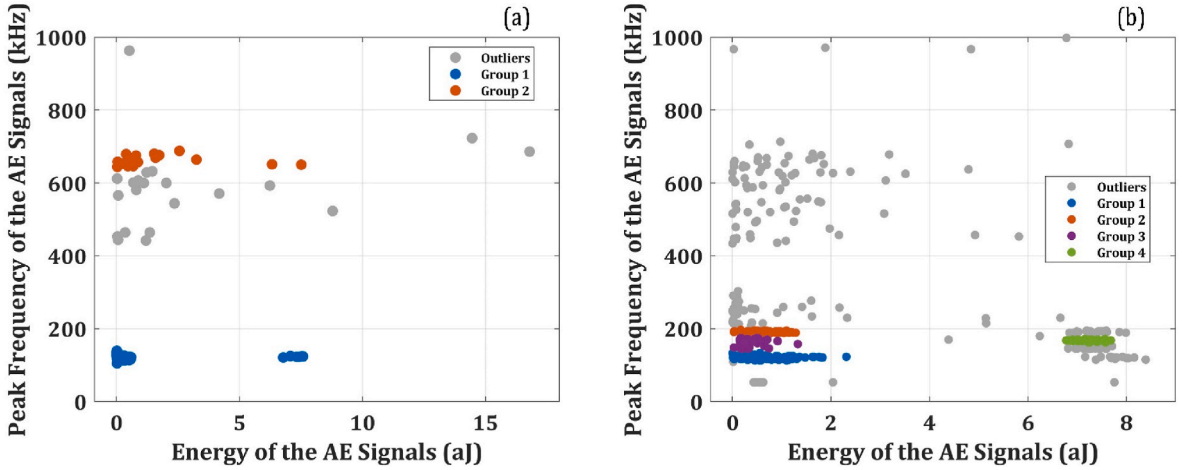

Fig. 7. AE Signal Features Clustered using DBSCAN (a) Signals generated from T-PET-G and (b) Signal generated from T-PU.

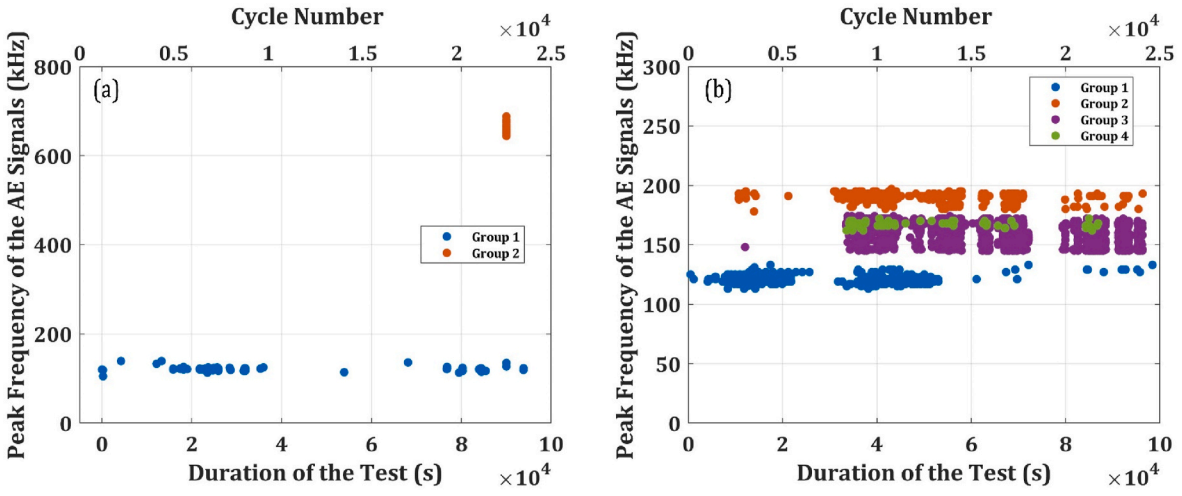

Fig. 8. Temporal Distribution of the Classified AE Signals represented as a function of their Peak Frequencies (a) from T-PET-G and (b) from T-PU.

initial phase indicates that the energy absorbed increases steadily due to the plastic deformation of the aligner. This can be attributed to the fact that the aligners are of thermoplastic materials, which are generally characterized by large plastic deformations. Particularly, the larger energy absorption in T-PU and AM-PU can be attributed to the softening of PU under cyclic loading (Qi and Boyce, 2005).

However, in a previous study, it was found that certain tooth positions of the aligner showed more deformation than the others during the cyclic loading (Casavola et al., 2022). Based on this, a hypothesis can be made. The energy absorbed by the aligner is more localized to certain teeth positions during the test. This may be the reason why the energy absorbed in T-PU and AM-PU decreases in the final phase of the test. In short, the energy absorbed by the aligners is localized to fewer tooth positions in the final phase, and thus, the energy drops.

Nevertheless, the trend in energy absorbed during the cyclic loading is different for all three aligners. For T-PET-G, there is no energy drop in the final phase of the test. It can be concurred that the energy absorbed during the cyclic loading of this aligner is uniformly distributed on the aligner surface during this phase. This can be attributed to the general strain behaviour of PET-G. Typically, PET-G are copolymers of PET and a glycol group. The presence of glycol group reduces the strain-induced crystallization, which allows the strain to be distributed (Dupaix and Boyce, 2005; Scetta et al., 2021). However, PU are two-phased copolymers that are characterized by the presence of soft and hard domains. During larger deformation, the presence of these dual domain may result in the nonuniform energy absorption by the material surface. For AM-PU, the energy absorbed increases in the initial phase and gradually decreases from the middle phase (from 9000 cycles; see Fig. 2 (a)). Thus, the energy is absorbed localized in this aligner from the middle phase. The results of T-PU, on the other hand, shows an interesting trend. The energy absorbed in this aligner gradually decreases in the middle phase (from 12500 cycles; see Fig. 2(a)) similar to AM-PU, but it drops suddenly at the beginning of the final phase (at cycle 16000). This clearly indicates that the locally absorbed energy by the T-PU is released in some form at this particular stage.

Considering the energy absorption behaviour of the CA, the increase stiffness of the aligners probably cannot be related to the damage state of the aligner, but rather to the strain hardening behaviour of their base materials. The presence of hard domains in PU is mainly due to the hydrogen bonds present in the polymer. They behave like physical crosslinks and influence the mechanical properties of the PU (Qi and Boyce, 2005). Extensive studies on the strain deformation behaviour of the PU under cyclic loading have demonstrated that its stiffness increases with time/cycle (Casavola et al., 2022; Kohda et al., 2013; Lombardo et al., 2015; Qi and Boyce, 2005; Tamburrino et al., 2020). This partially explains the increase in stiffness of the dental aligners. The general modulus of elasticity of PET-G is greater than that of PU. Consequently, the stiffnesses of T-PU and AM-PU (calculated from both slopes) in Fig. 2(b) and (c) are much lower than those of T-PET-G. As explained earlier, since the energy absorption is localized to a smaller

region of the aligner, the respective stiffness measured from the load-displacement curve may also represent the stiffness of this localized region. This could be the reason these aligners have different stiffness trends. Besides, for the orthodontic treatments, the aligners are expected to be fairly stiff over the cycle of utilization and all the three aligners have shown their compatibilities.

The localization of the energy and stiffness can also be concurred with the optical microscopy results in Section 3.2., where there are no localized damages are observed in T-PET-G in Fig. 3, while localized failures are observed in T-PU in Fig. 4.

To be precise, the energy absorbed in the T-PU is localized to a fewer tooth position (in this case to tooth 27). This localized damage position is possibly due to both the manufacturing defects and the strain behaviour of PU. As observed earlier, T-PU is characterized by large deformation. And the thermoforming process is known to induce thermal stress in the component. The large deformation and the residual thermal stress possibly resulted in the energy to be absorbed locally around the regions of microcracks formed during the manufacturing process. The absorbed energy reduced drastically as these cracks begin to propagate. From the energy curve of the T-PU, it can be concurred that this nucleation occurs approximately around 16000 cycles (see Fig. 2(a)). Apart from this localized damage, some other minor cracks and strain hardening regions are observed in some other tooth positions, which may have been originated from the thermoforming process.

In short, in T-PET-G, only minor damage can be observed (except for the chip removal in tooth 27 (see Fig. 4(d)) in different tooth positions, proving that the energy is not locally absorbed during the cyclic loading. Particularly in T-PU, most damages are localized in tooth 27.

In order to explicit these observations, the AE parameter- and frequency-based results need to be discussed. In T-PET-G, the cumulative counts of the AE events remain close to zero, indicating that there is no intense AE activity, up to cycle 4000 (Fig. 5(a)). In short, during the initial phase of the test, there is no intense AE activity. Soon after, it increases rapidly in a short span of time from 120 to 3200 before cycle 6000. This increase continues until cycle 9000, after which it stabilizes until the final phase of the test. After a prolonged period of cyclic loading, it increases again around cycle 18000 and continues up to cycle 20000. This indicates that there are distinguishable damage sources in T-PET-G during the cyclic loading. The first one occurs between cycles 4000 and 9000 and the second one between cycles 18000 and 20000. Now comparing these results to the optical microscopy results in Fig. 4, only two major damages can be observed: a major crack in tooth 14 (see Fig. 4(a)) and chip removal in tooth 27 (see Fig. 4(d)). Therefore, the two distinct damage sources seen in the cumulative counts of the AE signals can be directly related to these two damage modes. Nevertheless, the occurrence of these damage sources cannot be distinguished with the parameter-based AE data. To understand these damage sources, the frequency characteristics of the AE signals are examined. Fig. 6(a) and (b) shows the FFT results of the AE signals generated during the two periods indicated.

Both the AE signals from cycles 4000 to 9000 (Fig. 6(a)) and cycles 18000 to 20000 (Fig. 6(b)) share similar characteristics; their peak frequency centred around 150 kHz and most of the frequency components lie below 200 kHz. In addition, they share similar characteristics to the AE signals generated from the crack growth events from the preliminary test (see Fig. S3(b)). Particularly, the signal in Fig. 6(b) shares much similarity to that of Fig. S3(b). It must be remembered that the preliminary tests are designed specifically to generate AE signal from the crack growth events. Therefore, these AE signals can be directly related to the crack growth. (It should be noted that this analysis is carried out on a large number of signals, and for brevity, the FFTs of fewer signals are reported in this section). Now, comparing these results with the clustered signals based on their energy and peak frequency characteristics (in Fig. 7(a)), Group 1 signals have their peak frequencies between 100 kHz and 200 kHz. Their temporal distribution in Fig. 8(a) show that these signals start to appear around 4000 cycles and continues until the end of the test. The temporal distribution also shows that there are no signals between cycles 10000 and 18000, where the energy absorbed by the aligner remains the same. This confirms that the crack initiates at cycle 4000 and it continued until cycle 9000, then there was an idle period where the crack did not progress any further. It intensified after cycle 18000, albeit with much less influence on the energy absorption characteristics of the T-PET-G.

Group 2 signals in Fig. 7(a) have frequencies between 600 kHz and 700 kHz, which is quite unique in this case. It has been established that there are only two distinct damage modes: crack propagation and chip removal, as shown in Fig. 3. Group 2 signals can possibly be associated with the chip removal. However, considering their temporal distribution in Fig. 8(a), where they appeared at a very short instant, their source remains ambiguous. They could also be the frictional noise between the removed chip and the moving aligner casts. Nonetheless, the Group 2 signals have insignificant influence on the energy absorption characteristics of T-PET-G.

The cumulative counts of the AE signals generated by the T-PU are compared with their energy absorption characteristics and are reported in Fig. 5(b). The first significant difference between the AE results of T-PET-G and T-PU is the total number of cumulative counts recorded during the test. (Generally, the cumulative count number or cumulative energy between two different tests is not compared. However, given the huge difference in the cumulative count number, it is discussed here). The total number of cumulative counts in T-PET-G is only 5500 compared to 110000 in T-PU. The microscopy results of T-PU showed the presence of multiple cracks in tooth 27 (see Fig. 4(d)). It is, therefore, reasonable to assume that these crack lengths grew continuously during the cyclic test, thus generating continuous AE signals. It is clear from the cumulative counts in Fig. 5(b) that these cracks, however, did not initiate until in the first hour of loading, as they remain close to zero. A major crack begins to nucleate at cycle 2000 and it extended until cycle 5500, where it probably stopped growing further. This is evident from the cumulative counts, which remain stable until cycle 8000. After cycle 8000, there is a steady increase in the cumulative counts. This shows that, from this region, multiple cracks started to grow, and it continued until the end of the test. Comparing these results with the energy absorbed by this aligner is released through these cracks during the middle and final phases of the loading, as reported in Section 3.1.

To validate this observation, the frequency characteristics of the AE signals generated by the T-PU at different cycles are studied. The results are presented in Fig. 6(c) and (d). The FFT of both the signals presented in Fig. 6(c) and (d) shows similar frequency characteristics to those in Fig. 6(b). Their frequency components are centred around 150 kHz and most of their energy lies within 200 kHz frequency band. Therefore, it can be confirmed that the AE signals generated by the T-PU are from crack growth events, which can also be confirmed by the microscopy results (See Section 3.2).

Although all these signals are generated from the crack growth events, to identify their damage stages, the temporal distribution of the clustered AE signals are presented in Fig. 8(b). The results show the signals in Group 1 begin to appear at the early stages of loading, however, stop around 13000 cycles. Group 2 signals, on the other hand, begin to appear at 7500 cycles and stop at 16000 cycles. Cycle 16000 is of high significance, as the energy absorbed by the aligner dropped suddenly at this cycle. Group 2 signals stop appearing at this cycle, while only the signals from Group 3 follow them. This signifies that there were three separate damage stages represented by Groups 1, 2 and 3. The first one finishes at cycle 13000, while the last one continues even after the energy drop. The fewer number of signals in Group 4 renders them insignificant compared to Group 3 signals, which share similar frequency characteristics that appear around the same frequencies with different energies. Nonetheless, they can be associated with the same damage state as Group 3, however generating signals at a slightly higher energy (possibly due high strain energy release due to the crack nucleation). The microscopic images in Fig. 4(d) shows several localized

damages, confirming these observations.

All the hypotheses about the energy localizations in T-PET-G and T-PU are clearly validated by the microscopy and AE results. Furthermore, the different sources of damage, their initiation and termination are identified using the AE results. The different damage stages in the aligners are evaluated using the machine learning based clustering of the AE data. The overall performance of the three clear aligners is comprehensively studied using the optical microscopy and AE techniques.

5. Conclusion

In this study, three different aligners were tested under cyclic compression. Two thermoformed aligners of PU and PET-G and the popular additively manufactured Invisalign® (referred to as AM-PU in this study) were studied. The mechanical results, energy absorbed by the aligners and stiffness, showed that the energy was localised to fewer tooth positions in T-PU and AM-PU over a period of time, while there was no localisation in T-PET-G. T-PU suffered significant damage due to this localised energy absorption. AM-PU suffered very little damage despite the localised energy absorption. This is confirmed by the microscopic analysis and the AE results. The frequency-based study on the AE signals shows that most of the AE signals in T-PET-G and T-PU are from crack growth events, which are validated by the microscopy results. The machine learning-based AE analysis on the parameter-based and signal-based AE features identified the different damage progression stages in the aligners. T-PET-G undergoes a singular damage progression, although an ambiguous second damage state is observed for a brief moment in the temporal distribution. However, T-PU undergoes several damage progressions, which are explicitly classified by the clustered AE data.

Furthermore, the mechanical performances of these aligners are explained based on their manufacturing material. Thermoformed PU, unfortunately, did not perform well due to the presence of micro damages from the manufacturing process and the large deformation of the base material. On the other hand, thermoformed PET-G outperforms the commercially available Invisalign (AM-PU), despite having relatively lower energy absorption. However, improving the thermoforming process for the PU can potentially improve its mechanical performance. This remains open for future discussions.

Conflict of interest or competing interests

The authors declare that there is no conflict of interest in this work.

Data and code availability

The data used in this research work is a part of an ongoing research. It cannot be shared publicly. It is available upon request to the readers.

CRediT authorship contribution statement

Claudia Barile: Writing – review & editing, Validation, Methodology, Investigation. **Claudia Cianci:** Writing – review & editing, Writing – original draft, Validation, Methodology, Investigation, Formal analysis, Data curation, Conceptualization. **Vimalathithan Paramsamy Kannan:** Writing – review & editing, Writing – original draft, Validation, Software, Methodology, Investigation, Formal analysis, Data curation, Conceptualization. **Giovanni Pappalettera:** Writing – review & editing, Validation, Supervision, Methodology, Investigation, Conceptualization. **Carmine Pappalettere:** Conceptualization. **Caterina Casavola:** Resources. **Carmela Suriano:** Writing – review & editing, Resources. **Domenico Ciavarella:** Writing – review & editing, Supervision, Resources, Methodology, Conceptualization.

Declaration of competing interest

The authors declare that they have no known competing financial interests or personal relationships that could have appeared to influence the work reported in this paper.

Data availability

Data will be made available on request.

Acknowledgements

One of the Authors (*Vimalathithan Paramsamy Kannan*) acknowledges the support of the following:

Funder: Project funded under the National Recovery and Resilience Plan (PNRR), Mission 4 Component 2 Investment 1.4 - Call for tender No. 3138 of December 16, 2021 of Italian Ministry of University and Research funded by the European Union – NextGenerationEU.

Award Number: CNMS MOST, Concession Decree No. 1033 of June 17, 2022 adopted by the Italian Ministry of University and Research, CUP: D93C22000410001, Spoke 14" Hydrogen and New Fuels".

One of the Authors *(Cianci Claudia)* acknowledges that this work was partly supported by the Italian Ministry of University and Research under the Programme "Department of Excellence" Legge 232/2016 (Grant No. CUP - D93C23000100001)".

Appendix A. Supplementary data

Supplementary data to this article can be found online at https://doi.org/10.1016/j.jmbbm.2024.106451.

References

Abásolo, D., Hornero, R., Gómez, C., García, M., López, M., 2006. Analysis of EEG background activity in Alzheimer's disease patients with Lempel–Ziv complexity and central tendency measure. Med. Eng. Phys. 28, 315–322.

Aboy, M., Hornero, R., Abásolo, D., Álvarez, D., 2006. Interpretation of the Lempel-Ziv complexity measure in the context of biomedical signal analysis. IEEE Trans. Biomed. Eng. 53, 2282–2288.

Aggelis, D.G., Kordatos, E.Z., Matikas, T.E., 2011. Acoustic emission for fatigue damage characterization in metal plates. Mech. Res. Commun. 38, 106–110.

Albilali, A.T., Baras, B.H., Aldosari, M.A., 2023. Evaluation of mechanical properties of different thermoplastic orthodontic retainer materials after thermoforming and Thermocycling. Polymers 15, 1610.

Andjela, L., Abdurahmanovich, V.M., Vladimirovna, S.N., Mikhailovna, G.I., Yurievich, D.D., Alekseevna, M.Y., 2022. A review on Vat Photopolymerization 3D-printing processes for dental application. Dent. Mater.

Baker, C., Morscher, G.N., Pujar, V.V., Lemanski, J.R., 2015. Transverse cracking in carbon fiber reinforced polymer composites: modal acoustic emission and peak frequency analysis. Compos. Sci. Technol. 116, 26–32.

Barile, C., Casavola, C., Pappalettera, G., Kannan, V.P., 2023. Interpreting the Lempel–Ziv complexity of acoustic emission signals for identifying damage modes in composite materials. Struct. Health Monit. 22, 1708–1720.

Barile, C., Casavola, C., Pappalettera, G., Kannan, V.P., 2020. Application of different acoustic emission descriptors in damage assessment of fiber reinforced plastics: a comprehensive review. Eng. Fract. Mech. 235, 107083.

Barile, C., Casavola, C., Pappalettera, G., Vimalathithan, P.K., 2019. Damage characterization in composite materials using acoustic emission signal-based and parameter-based data. Compos. B Eng. 178, 107469.

Barone, S., Paoli, A., Neri, P., Razionale, A.V., Giannese, M., 2017. Mechanical and Geometrical properties assessment of thermoplastic materials for biomedical application. In: Advances on Mechanics, Design Engineering and Manufacturing: Proceedings of the International Joint Conference on Mechanics, Design Engineering & Advanced Manufacturing (JCM 2016), 14-16 September, 2016. Springer, Catania, Italy, pp. 437–446.

Boyd, R.L., Miller, R.J., Vlaskalic, V., 2000. The Invisalign system in adult orthodontics: mild crowding and space closure cases. J. Clin. Orthod. 34, 203–212.

Burud, N.B., Kishen, J.M.C., 2021. Response based damage assessment using acoustic emission energy for plain concrete. Constr Build Mater 269, 121241.

Buttke, T.M., Proffit, W.R., 1999. Referring adult patients for orthodontic treatment. J. Am. Dent. Assoc. 130, 73–79.

Casavola, C., Pappalettera, G., Pappalettere, C., Patronelli, M., Renna, G., Laurenziello, M., Ciavarella, D., 2022. A full-field DIC analysis of the mechanical-deformation behavior of polyethylene terephthalate glycol (PET-G) aligners. J. Mech. Behav. Biomed. Mater. 134, 105391.

Cianci, C., Pappalettera, G., Renna, G., Casavola, C., Laurenziello, M., Battista, G., Pappalettere, C., Ciavarella, D., 2020. Mechanical behavior of PET-G tooth aligners under cyclic loading. Front Mater 7, 104.
Gusev, V.D., Nemytikova, L.A., Chuzhanova, N.A., 1999. On the complexity measures of genetic sequences. Bioinformatics 15, 994–999.
Dupaix, R.B., Boyce, M.C., 2005. Finite strain behavior of poly (ethylene terephthalate) (PET) and poly (ethylene terephthalate)-glycol (PETG). Polymer (Guildf) 46, 4827–4838.
Duyck, J., Van Oosterwyck, H., Vander Sloten, J., De Cooman, M., Puers, R., Naert, I., 2000. Magnitude and distribution of occlusal forces on oral implants supporting fixed prostheses: an in vivo study. Clin. Oral Implants Res. 11, 465–475.
Eliades, T., Bourauel, C., 2005. Intraoral aging of orthodontic materials: the picture we miss and its clinical relevance. Am. J. Orthod. Dentofacial Orthop. 127, 403–412.
Elkholy, F., Schmidt, S., Schmidt, F., Amirkhani, M., Lapatki, B.G., 2021. Force decay of polyethylene terephthalate glycol aligner materials during simulation of typical clinical loading/unloading scenarios. Journal of Orofacial Orthopedics/Fortschritte der Kieferorthopadie.
Ereifej, N., Silikas, N., Watts, D.C., 2008. Initial versus final fracture of metal-free crowns, analyzed via acoustic emission. Dent. Mater. 24, 1289–1295.
Ester, M., Kriegel, H.-P., Sander, J., Xu, X., 1996. A density-based algorithm for discovering clusters in large spatial databases with noise. In: Kdd, pp. 226–231.
Fang, D., Zhang, N., Chen, H., Bai, Y., 2013. Dynamic stress relaxation of orthodontic thermoplastic materials in a simulated oral environment. Dent. Mater. J. 32, 946–951.
Gibbs, C.H., Mahan, P.E., Lundeen, H.C., Brehnan, K., Walsh, E.K., Holbrook, W.B., 1981. Occlusal forces during chewing and swallowing as measured by sound transmission. J. Prosthet. Dent 46, 443–449.
Gillis, P.P., 1972. Dislocation motions and acoustic emissions. In: Acoustic Emission. ASTM International.
Gunatillake, P.A., Martin, D.J., Meijs, G.F., McCarthy, S.J., Adhikari, R., 2003. Designing biostable polyurethane elastomers for biomedical implants. Aust. J. Chem. 56, 545–557.
Hamstad, M.A., 2000. Thirty years of advances and some remaining challenges in the application of acoustic emission to composite materials. Acoustic emission beyond the millennium 77–91.
Huang, J., Zhang, Z., Zheng, B., Qin, R., Wen, G., Cheng, W., Chen, X., 2023. Acoustic emission technology-based multifractal and unsupervised clustering on crack damage monitoring for low-carbon steel. Measurement 217, 113042.
Iijima, M., Kohda, N., Kawaguchi, K., Muguruma, T., Ohta, M., Naganishi, A., Murakami, T., Mizoguchi, I., 2015. Effects of temperature changes and stress loading on the mechanical and shape memory properties of thermoplastic materials with different glass transition behaviours and crystal structures. Eur. J. Orthod. 37, 665–670.
Kohda, N., Iijima, M., Muguruma, T., Brantley, W.A., Ahluwalia, K.S., Mizoguchi, I., 2013. Effects of mechanical properties of thermoplastic materials on the initial force of thermoplastic appliances. Angle Orthod. 83, 476–483.
Kravitz, N.D., Kusnoto, B., BeGole, E., Obrez, A., Agran, B., 2009. How well does Invisalign work? A prospective clinical study evaluating the efficacy of tooth movement with Invisalign. Am. J. Orthod. Dentofacial Orthop. 135, 27–35.
Lesser, A.J., 1995. Changes in mechanical behavior during fatigue of semicrystalline thermoplastics. J. Appl. Polym. Sci. 58, 869–879.
Li, H., Li, J., Yun, X., Liu, X., Fok, A.S.-L., 2011. Non-destructive examination of interfacial debonding using acoustic emission. Dent. Mater. 27, 964–971.
Liptai, R.G., Harris, D.O., Tatro, C.A., 1972. An introduction to acoustic emission. Acoustic Emission 505.
Lombardo, L., Arreghini, A., Maccarrone, R., Bianchi, A., Scalia, S., Siciliani, G., 2015. Optical properties of orthodontic aligners—spectrophotometry analysis of three types before and after aging. Prog. Orthod. 16, 1–8.
Lombardo, L., Martines, E., Mazzanti, V., Arreghini, A., Mollica, F., Siciliani, G., 2016. Stress relaxation properties of four orthodontic aligner materials: a 24-hour in vitro study. Angle Orthod. 87, 11–18.
Ohno, K., Ohtsu, M., 2010. Crack classification in concrete based on acoustic emission. Constr Build Mater 24, 2339–2346.
Papadopoulou, A.K., Cantele, A., Polychronis, G., Zinelis, S., Eliades, T., 2019. Changes in roughness and mechanical properties of Invisalign® appliances after one-and two-weeks use. Materials 12, 2406.
Pinchuk, L., 1995. A review of the biostability and carcinogenicity of polyurethanes in medicine and the new generation of'biostable'polyurethanes. J. Biomater. Sci. Polym. Ed. 6, 225–267.
Porojan, L., Toma, F.R., Bîrdeanu, M.I., Vasiliu, R.D., Matichescu, A., 2023. Topographical and optical characteristics of thermoplastic dental appliances materials related to water sorption. J. Funct. Biomater. 14, 190.
Qi, H.J., Boyce, M.C., 2005. Stress–strain behavior of thermoplastic polyurethanes. Mech. Mater. 37, 817–839.
Quinzi, V., Orilisi, G., Vitiello, F., Notarstefano, V., Marzo, G., Orsini, G., 2023. A spectroscopic study on orthodontic aligners: first evidence of secondary microplastic detachment after seven days of artificial saliva exposure. Sci. Total Environ. 161356.
Radhakrishnan, N., Gangadhar, B.N., 1998. Estimating regularity in epileptic seizure time-series data. IEEE Eng. Med. Biol. Mag. 17, 89–94.
Rossini, G., Parrini, S., Castroflorio, T., Deregibus, A., Debernardi, C.L., 2015. Efficacy of clear aligners in controlling orthodontic tooth movement: a systematic review. Angle Orthod. 85, 881–889.
Ryu, J.-H., Kwon, J.-S., Jiang, H.B., Cha, J.-Y., Kim, K.-M., 2018. Effects of thermoforming on the physical and mechanical properties of thermoplastic materials for transparent orthodontic aligners. The Korean Journal of Orthodontics 48, 316–325.
Saeedifar, M., Zarouchas, D., 2020. Damage characterization of laminated composites using acoustic emission: a review. Compos. B Eng. 195, 108039.
Sander, J., Ester, M., Kriegel, H.-P., Xu, X., 1998. Density-based clustering in spatial databases: the algorithm gdbscan and its applications. Data Min. Knowl. Discov. 2, 169–194.
Scetta, G., Ju, J., Selles, N., Heuillet, P., Ciccotti, M., Creton, C., 2021. Strain induced strengthening of soft thermoplastic polyurethanes under cyclic deformation. J. Polym. Sci. 59, 685–696.
Schuster, S., Eliades, G., Zinelis, S., Eliades, T., Bradley, T.G., 2004. Structural conformation and leaching from in vitro aged and retrieved Invisalign appliances. Am. J. Orthod. Dentofacial Orthop. 126, 725–728.
Schwitalla, A.D., Spintig, T., Kallage, I., Müller, W.-D., 2015. Flexural behavior of PEEK materials for dental application. Dent. Mater. 31, 1377–1384.
Tak, S., Jeong, Y., Kim, J.-E., Kim, J.-H., Lee, H., 2023. A comprehensive study on the mechanical effects of implant-supported prostheses under multi-directional loading and different occlusal contact points. BMC Oral Health 23, 338.
Tamburrino, F., D'Antò, V., Bucci, R., Alessandri-Bonetti, G., Barone, S., Razionale, A.V., 2020. Mechanical properties of thermoplastic polymers for aligner manufacturing: in vitro study. Dent. J. 8, 47.
Vallittu, P.K., 2002. Use of woven glass fibres to reinforce a composite veneer. A fracture resistance and acoustic emission study. J. Oral Rehabil. 29, 423–429.
Wang, C., Hausberger, A., Berer, M., Pinter, G., Grün, F., Schwarz, T., 2019. Fretting behavior of thermoplastic polyurethanes. Lubricants 7, 73.
Zhang, N., Bai, Y., Ding, X., Zhang, Y., 2011. Preparation and characterization of thermoplastic materials for invisible orthodontics. Dent. Mater. J. 30, 954–959.